coatings

MDPI

Article

Flexible Free-Standing Graphene-Fe_2O_3 Hybrid Paper with Enhanced Electrochemical Performance for Rechargeable Lithium-Ion Batteries

Chuanning Yang [1,2,3,*], Wangchuan Xiao [1,3], Shizhao Ren [1] and Qiyong Li [1]

[1] School of Resource and Chemical Engineering, Sanming University, Sanming 365004, China
[2] Science and Technology, Sanming Institute of the Fluorochemical Industry, Sanming 365004, China
[3] Fujian Fluoine Based Chemical Engineering Service Platform of Science and Technology Combined with Economy, Sanming University, Sanming 365004, China
* Correspondence: yangcn@fjsmu.edu.cn

Abstract: The cyclic performance of flexible free-standing graphene-Fe_2O_3 hybrid sheet is considerably improved and was fabricated by a novel one-step hydrothermal process. The X-ray diffraction (XRD), X-ray photoelectron spectroscopy (XPS), thermogravimetric (TGA), scanning electron microscopy (SEM), transmission electron microscopy (TEM), and electrochemical workstation are performed to characterize the microstructure and electrochemical performance of the graphene-Fe_2O_3 hybrid sheet. At a current density of 200 $mA{\cdot}g^{-1}$, the obtained product has a high initial discharge capacity of 1466 $mAh{\cdot}g^{-1}$. The nanohybrids also exhibited a considerably high reversible capacity of 765 $mAh{\cdot}g^{-1}$ and high Coulombic efficiency of 99.8% after 100 cycles, which benefited from the open 3D laminated nanostructure constructed by layered graphene paper and Fe_2O_3 nanoparticles. Therefore, the composite has excellent rate performance and stability and can be greatly extended as the anode material of lithium-ion batteries.

Keywords: graphene; nanostructure; lithium-ion batteries; Fe_2O_3; anodes; flexible

Citation: Yang, C.; Xiao, W.; Ren, S.; Li, Q. Flexible Free-Standing Graphene-Fe_2O_3 Hybrid Paper with Enhanced Electrochemical Performance for Rechargeable Lithium-Ion Batteries. *Coatings* **2022**, *12*, 1726. https://doi.org/10.3390/coatings12111726

Academic Editor: Vitaly Tseluikin

Received: 11 October 2022
Accepted: 8 November 2022
Published: 11 November 2022

1. Introduction

Owing to the increasing demands for flexible energy, storing devices on account of lithium-ion batteries (LIBs) have been used as green power resources, which have aroused tremendous attention in the field of new electrochemical energy storage [1]. Graphene is a special carbon material, which owns one layer of two-dimensional carbon atom structure, and recently, it has become an area of current research focus due to its brilliant electrochemical property [2], supreme electronic conductivity [3], extraordinary structural flexibility and superhigh specific surface area [4], and it could be an ideal substrate for embedding functional substances [5]. Graphene paper (GP) and its different kinds of derivatives have been successfully prepared by filtrating graphene nanosheets and are directly used as the electrode materials of flexible energy storage devices without any conductive additives and binder [6]. The free-standing GP and its various derivatives electrodes can improve the electrical conductivity and achieve higher active material-to-substrate mass ratios compared with the traditional electrodes [7].

Graphene has remarkable properties, but the inevitable aggregation of individual graphene layers impedes its application in high-performance energy because of the existence of the van der Waals attraction during graphene assemblies [8]. Plenty of methods have been investigated to overcome the barrier by adding various types of hard or soft pillars, such as carbon black [9], carbon nanotube [10], curly graphene nanosheets [11], and solvent molecules [12]. Especially by using solvent molecules, a self-assembly, solvent graphene (SSG) paper can be prevented from restacking and show excellent electrochemical performance [13].

It is known that the GP with a sandwich structure displays a large specific area, and the electrodes of LIBs may generate solid electrolyte interface (SEI) films, which leads to a big irreversible capacity and worse cyclic stability [14]. For achieving high capacity and excellent electrochemical performance, some other functional materials, such as transition metal oxides, can be anchored on the surface of graphene sheets to form paper-like flexible electrodes [15]. A flexible 3D network nanostructure constructed by graphene sheets can not only serve as the skeleton for the integration of heterogeneous nanostructured transition metal oxides but also provide a void space buffer for the volume changes of the metal oxide nanoparticles during the Li^+ insertion and extraction of the charge-discharge process [16]. Moreover, as the conductive substrate, the graphene network nanostructure can promote the rate performance owing to its brilliant electric conductivity [17]. Thus, flexible graphene/Fe_3O_4 papers [18], sandwich-like graphene/ZnO [19], graphene/MnO_2 nanostructured paper [20], and graphene/Fe_2O_3 hybrid papers [21] as the electrochemical capacitor electrodes and magnetic-controlled switches have been studied. On the other hand, all these flexible graphene hybrid sheets mentioned above, which were generally fabricated from graphene oxide (GO) and precursors of the transition metal oxide, showed relatively low oxide loading on the graphene nanosheets and not optimal electrochemical performance [22]. Therefore, it is difficult to prepare well-dispersed graphene solution with the precursors of the transition metal oxide to form flexible paper-like hybrids [23] because when the metal ion salts were added into the graphene solution, it caused instant coacervation of the mixed solution [24].

Therefore, to overcome the shortcoming mentioned above, we provide a reliable and novel ex situ way to fabricate the flexible free-standing graphene-Fe_2O_3 hybrid sheet with a high mass loading of metal oxides. Specifically, wet graphene paper is fabricated by filtrating the well-diversified graphene solution, immersing it into the precursor of Fe_2O_3 solution, then Fe_2O_3 is loaded into the GP to form a 3D open structure with good flexibility and geometry. The obtained flexible graphene-Fe_2O_3 hybrid paper can be directly used as the anode materials of LIBs without adding any current collectors, binders, or additives. Meanwhile, flexible graphene-Fe_2O_3 hybrid paper with 3D nanostructure shows excellent physical and electrochemical performance as the paper electrode for new energy-storing devices.

2. Materials and Methods

2.1. Materials Preparation

All reagents were analytical grade and were not further purified in the experiment. The graphene-Fe_2O_3 hybrid sheet was synthesized as follows:

Natural flake graphite powder (Sigma-Aldrich, Shenyang, China) was used to prepare the graphene solution, which was mentioned in our previous work [25], and 15 mL sodium dodecyl sulfate (SDS)was added into the prepared graphene solution of 80 mL (~0.09 g/L) under the ultra-sonication treatment (750 W, 66% amplitude, Sigma-Aldrich, Shenyang, China) for 2 h. After that, the wet papers were obtained by filtrating the above mixed solution. The precursor solution of Fe_2O_3 was prepared by mixing 3 mmol $FeSO_4 \cdot 7H_2O$, 5.4 g urea, 30 mL deionized water (DIW) (Sigma-Aldrich, Shenyang, China), and 15 mL ethanol (Sigma-Aldrich, Shenyang, China) under the ultra-sonication treatment for 30 min. Then, the wet papers were dipped into the precursor solution of Fe_2O_3 for 2 h. The mixture was then transferred to a Teflon-lined autoclave and hydrothermal heated at 160 °C for 10 h. The finally acquired hydrothermal product of graphene-Fe_2O_3 hybrid paper was collected and washed with DIW and ethanol several times after cooling to room temperature and then followed by vacuum drying overnight at 30 °C. The reference $Fe_2O_3$was fabricated with the same process, and no graphene solution was added.

2.2. Materials Characterization

The microstructure and morphology of graphene-Fe_2O_3 hybrid sheet were characterized by various techniques. XRD (DMAX-Ultima IV, Rigaku Corporation, Tokyo, Japan)

measurement was utilized to determine the crystal structure of the samples. The microstructure and morphology of the samples were acquired by using the TEM (JEM-ARM200F, JEOL, Tokyo, Japan) and SEM (Ultra Plus, Zeiss, Oberkochen, Germany). To identify the Fe_2O_3 mass loading of the graphene-Fe_2O_3 hybrid sheet, the TGA (SDT 2960, TA Instruments, New Castle, DE, USA) was employed with the temperature range from room temperature to 900 °C with a heating rate of 20 °C/min. Furthermore, the functional groups of the samples were determined by XPS (K-Alpha, Thermo Fisher Scientific, Waltham, MA, USA).

2.3. Electrochemical Analysis

The CR2032 coin cell structure was used to study the electrochemical properties of the hybrid sheet. In the absence of binder and carbon black, the working electrode was prepared from a graphene-Fe_2O_3 hybrid sheet. The reference Fe_2O_3 anode was prepared by commingling the as-prepared Fe_2O_3, polyvinylidene difluoride (PVDF) (Sigma-Aldrich, Shenyang, China) and carbon black (Sigma-Aldrich, Shenyang, China) in N-methylpyrrolidone (NMP) (Sigma-Aldrich, Shenyang, China) at a proportion of 80:10:10 by weight. Lithium metal foil was used as the counter electrode and 1 M LiPF6 as electrolyte; the CR2032 coin battery was dissolved by volume in a mixture of 1:1 diethyl carbonate (DEC) (Sigma-Aldrich, Shenyang, China) and ETH-alkyne carbonate (EC) (Sigma-Aldrich, Shenyang, China) in Celgard separator 2340 and assembled in a glove box (Sigma-Aldrich, Shenyang, China) filled with argon gas. All electrochemical tests were measured at room temperature. The electrochemical performance of the anodes was tested in a LAND CT-2001A system (Sigma-Aldrich, Shenyang, China) with voltages ranging from 0.01 to 3.0 V vs. Li^+/Li. The electrochemical impedance spectroscopy (EIS) and cyclic voltammetry (CV) curve of the cell were acquired by an electrochemical workstation (PGSTAT100N, Autolab, Helishaw, Swiss).

3. Results

Figure 1 displays the fabrication process of flexible free-standing graphene-Fe_2O_3 hybrid sheet. Particularly, sodium dodecyl sulfate (SDS) was added in the solution of graphene can not only act as a molecular template that controls nucleation and growth of the Fe_2O_3 nanoparticles but also serve as prop to provide enough space between the graphene layers to hold sufficient ferrous sulfate (Fe_2SO_4), the precursor of Fe_2O_3, during the process of dipping. The Fe_2O_3 nanoparticles were formed during the hydrothermal treatment and evenly anchored on the surface of the graphene. Finally, five graphene-Fe_2O_3 hybrid sheets were obtained for further investigation. The characterization and electrochemical analysis proceeded to verify the potential application prospect of the samples.

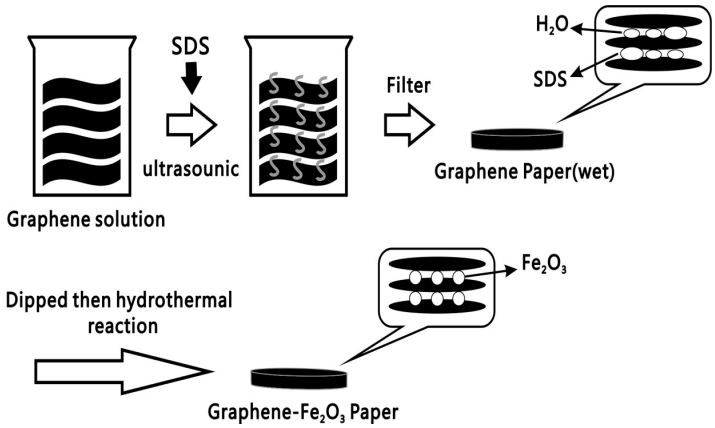

Figure 1. The schematic illustration of the synthesis process of graphene-Fe_2O_3 sheet.

The XRD measurement is used to ascertain the crystallographic phases of the products. The XRD pattern of the graphene-Fe_2O_3 sheet is shown in Figure 2. The diffraction peaks located at 2θ = 28.63°, 38.89°, 42.02°, 48.30°, 58.29°, 63.99°, 74.26°, 76.55°, 83.39°, and

86.52° can correspond to (012), (104), (110), (113), (024), (116), (214), (300), (208), and (1010) planes of the α-Fe_2O_3 (JCPDS 33-0664). Meanwhile, the diffraction peaks located at 2θ = 24.06° can correspond to (105) planes of the γ-Fe_2O_3 (JCPDS 25-1402). Therefore, both maghemite γ-Fe_2O_3 and hematite α-Fe_2O_3 crystal structures coexist in the products. The sharp diffraction peaks indicate the good crystallization of Fe_2O_3 during the hydrothermal process, and there is no obvious impurity [25].

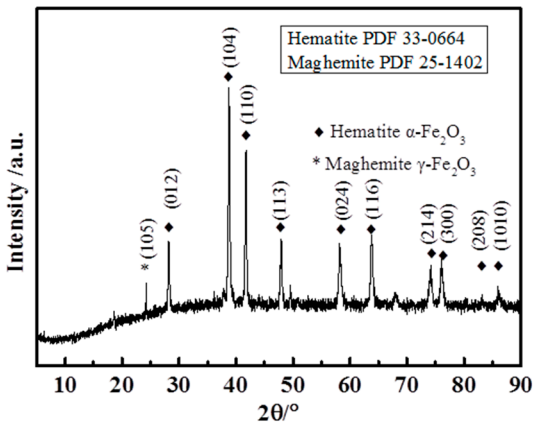

Figure 2. The XRD pattern of graphene-Fe_2O_3 sheet.

The weight ratio of Fe_2O_3 nanoparticles in graphene-Fe_2O_3 sheet is determined by thermogravimetric (TGA) measurements. Figure 3 shows the TGA curves of graphene-Fe_2O_3 sheet. The TGA measurement identified the weight loss of TGA measurements from room temperature to 800 °C. The 5% weightlessness of the samples below 250 °C is primarily due to the removal of SDS and moisture on the surface of the graphene-Fe_2O_3 sheet. There is a rapid weight loss evidently appearing at a temperature range of 250–400 °C for the reason of the consumption of graphene and dehydration of oxides. After reaching 650 °C, the loading of Fe_2O_3 in the graphene-Fe_2O_3 sheet resulting in 70.65% is stable with no further weight loss, indicating the triumphant synthesis of the sheet with a high mass loading of metal oxides [25].

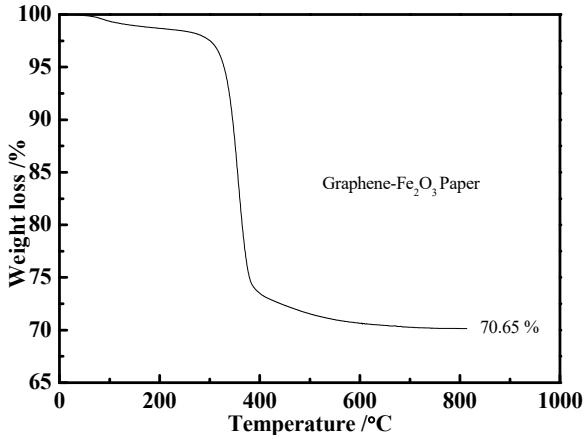

Figure 3. The TGA pattern of the hybrid graphene-Fe_2O_3 paper.

XPS measurement was employed to further investigate the elemental components of graphene-Fe_2O_3 hybrid sheet. The full scanning spectrum of graphene-Fe_2O_3 hybrid paper is shown in Figure 4a, which reveals Fe, O, and C elements existed in the graphene-Fe_2O_3 hybrid sheet. The atomic ratios of Fe, O, and C are 14.63%, 36.82%, and 48.54%, respectively. It can be apparently observed that the strong signals of Fe 2p, O 1s, and C 1s were detected on the products. The spectra of graphene-Fe_2O_3 hybrid sheet coincide with the binding energies of Fe 2p are shown in Figure 4b. It shows that the photoelectron peaks at 710.8 and

724.3 eV were assigned to the binding energies of Fe $2p_{1/2}$ and Fe $2p_{3/2}$, which is well matched with previous literature and verifying the results of XRD. In the meantime, the binding energy of O 1s is shown in Figure 4c, the peak at 532.1 eV is attributed to the surface OH groups and chemisorbed oxygen, and the peak at 530.4 is relative to the oxygen in an oxygen vacant environment. Meanwhile, the peak at 528.3 eV represents the O^{2-} in the Fe_2O_3. The high-resolution XPS peaks of C 1s spectra of the graphene-Fe_2O_3 hybrid sheet are shown in Figure 4d. The peaks at 284.2 eV and 285.6 eV confirm the presence of C=C and C-OH. The peaks at 288.3 and 287.9 eV indicate the presence of C=O, which is owing to the groups of carboxylic acids and carbonyl carbon [25]. All these results further indicate the successful fabrication of graphene-Fe_2O_3 hybrid sheet.

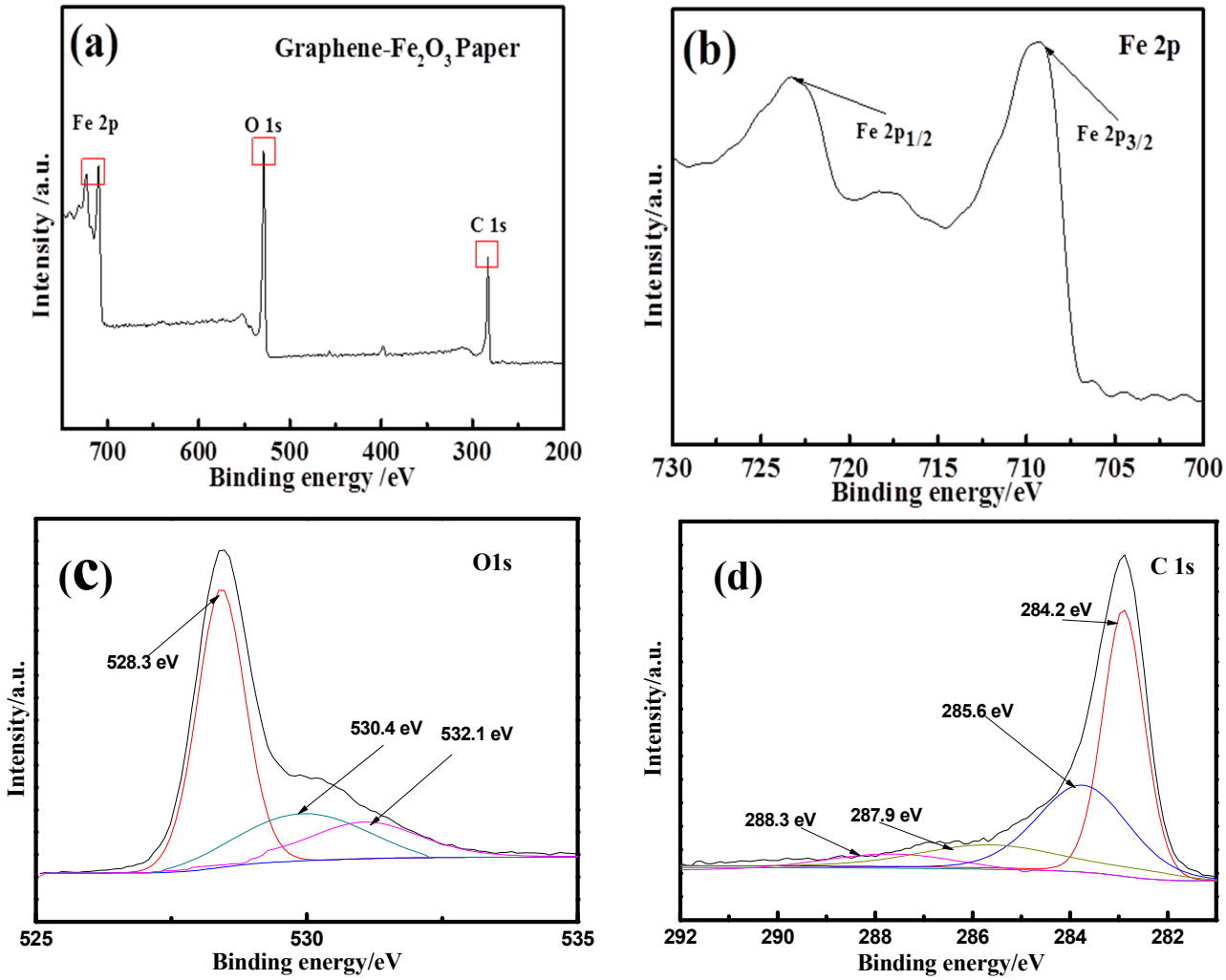

Figure 4. The XPS curves of hybrid flexible sheet (**a**) XPS spectra of the hybrid graphene-Fe_2O_3 sheet and the homologous high-resolution spectra of (**b**) Fe 2p, (**c**) O 1s, and (**d**) C 1s.

The morphology and microstructure of graphene-Fe_2O_3 hybrid paper were investigated by SEM and TEM. The cross-section of the graphene-Fe_2O_3 sheet and pure graphene paper, which were prepared by filtering the same quantity of graphene solution, is shown in Figure 5a,b, respectively. It is obviously observed that the thickness of graphene-based sheets increased from about 3.75 to 12.6 μm owing to the insertion of Fe_2O_3 nanoparticles between the layered graphene sheet [26]. The enlarged space of an open 3D laminated structure of graphene-Fe_2O_3 hybrid sheet provides the electron transfer and ion transport path, which is available for Li-ion insertion/extraction, even at high rates [27].

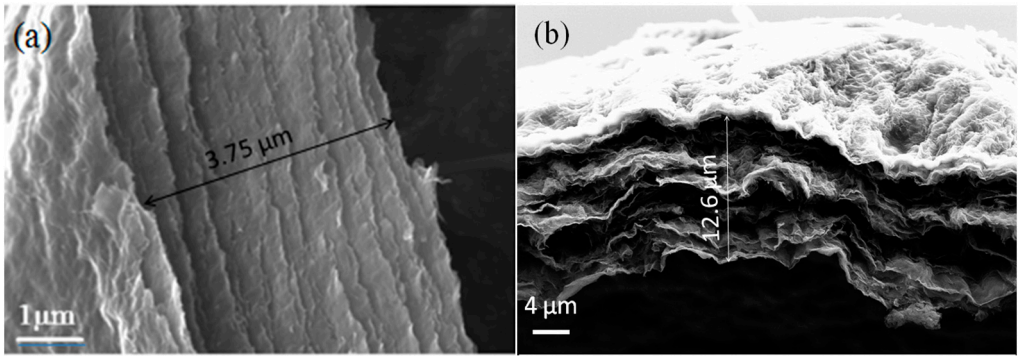

Figure 5. The SEM pictures of the cross-section of (**a**) the pure graphene sheet and (**b**) the graphene-Fe_2O_3 sheet.

The microstructure of graphene-Fe_2O_3 hybrid sheet was further studied by means of TEM. Fe_2O_3 nanoparticles with a diameter of about 20 nm are diffused among the layered graphene substrates were shown in Figure 6a. The high-resolution TEM (HR-TEM) image of the graphene-Fe_2O_3 hybrid sheet, as shown in Figure 6b, displays lattice fringes with a spacing of 0.221 nm and 0.184 nm separately, which correspond with the (113) and (024) planes of Fe_2O_3 nanoparticles, respectively.

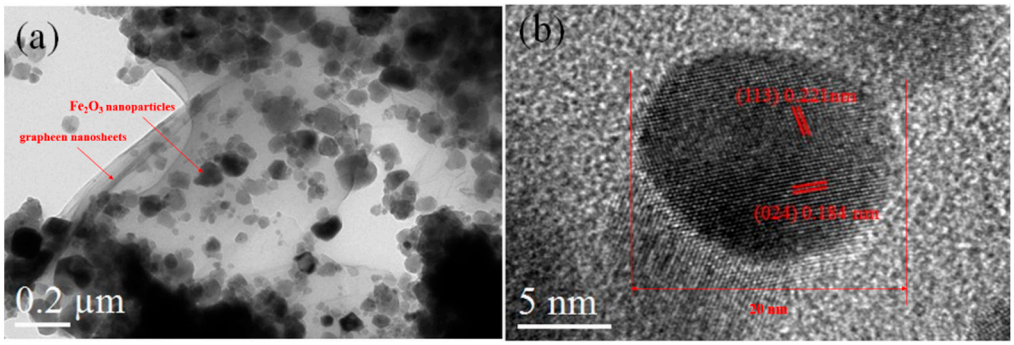

Figure 6. TEM pictures of hybrid flexible paper (**a**) The TEM picture and (**b**) the high-resolution TEM picture of graphene-Fe_2O_3 sheet.

The graphene-Fe_2O_3 hybrid sheet with novel 3D laminated microstructure enhance the cyclic stability and the rate of Li-ion insertion/extraction utilized as anodes for high-power LIBs. To further verify the potential application of graphene-Fe_2O_3 hybrid sheet electrodes, the free-standing hybrid papers were directly used as the anodes of LIBs and assembled in the coin cells.

The electrochemical behavior of graphene-Fe_2O_3 hybrid sheet as electrode for LIBs was investigated by cyclic voltammograms (CV). The CV curve of graphene-Fe_2O_3 sheet anode is exhibited in Figure 7a for the 1st, 2nd, and 3rd were investigated at a scan rate of 0.5 $mV{\cdot}s^{-1}$ with a voltage range from 0.01 to 3.0 V. During the first cycle, peaks at 1.42 V, 0.75 V, and 0.35 V are relevant to the stepwise reduction of Fe^{3+} to Fe^{2+} and Fe and the formation of SEI film, respectively. During the delithium process, two oxidation peaks at about 1.89 V and 2.01 V may be attributed to the oxidation of Fe back to Fe^{3+} [27,28]. In the following scans, the peaks at lower potentials vanish, indicating the generation of the SEI appeared at the first cycle, and all other voltage peaks shift to higher potentials [27]. Furthermore, the CV curves anastomose with the following cycles perfectly after the second cycle, manifesting the better electrochemical reversibility of the graphene-Fe_2O_3 hybrid sheet electrode [27].

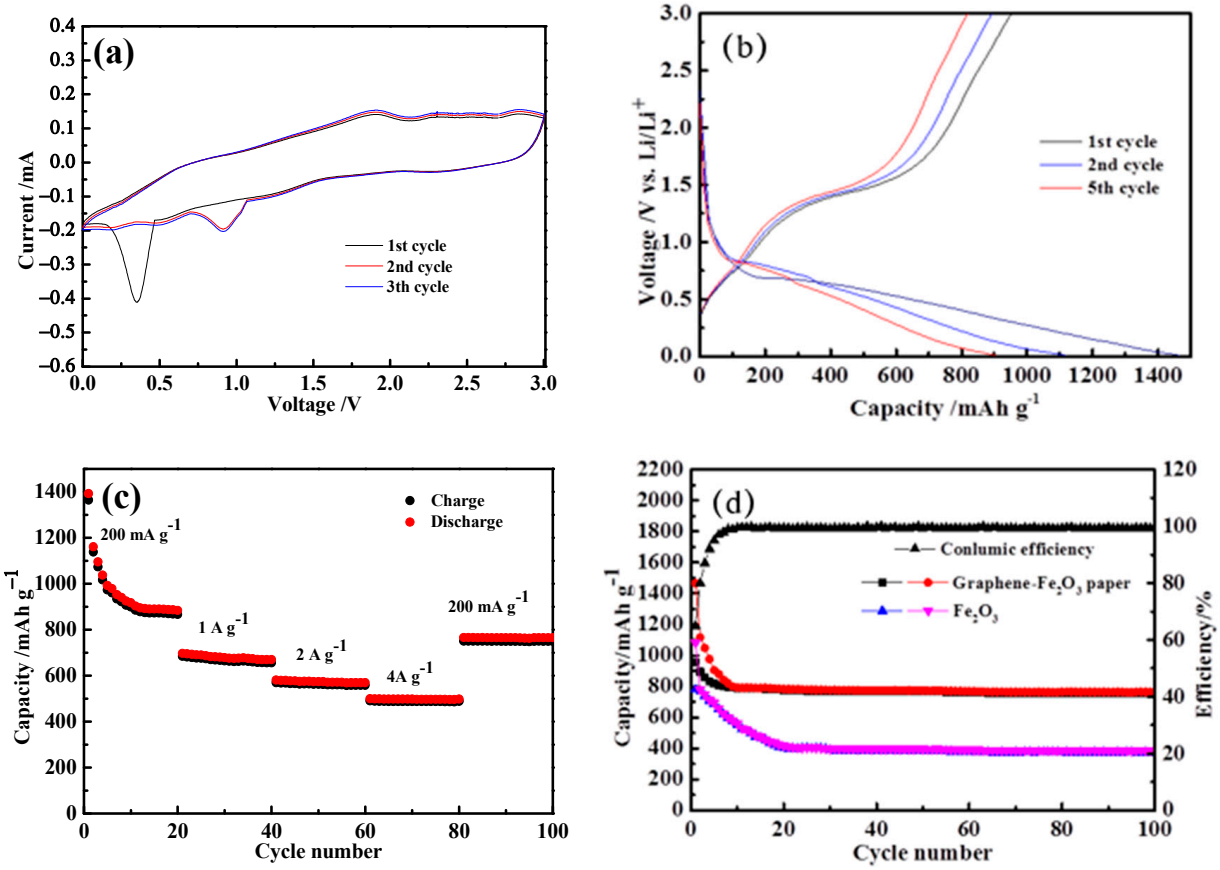

Figure 7. The electrochemical property of the obtained samples as the anode for LIBs; (**a**) CV curves of the graphene-Fe_2O_3 sheet electrode at a scan rate of 0.5 $mV \cdot s^{-1}$; (**b**) the charge-discharge voltage curves of the graphene-Fe_2O_3 sheet electrode at the current density of 200 $mA \cdot g^{-1}$ for the cycle of 1st, 2nd, and 5th; (**c**) the rate capabilities of the graphene-Fe_2O_3 sheet anodes at the current densities ranging from 0.2 to 4.0 $A \cdot g^{-1}$; (**d**) the cycle performance and Coulombic efficiency of the graphene-Fe_2O_3 sheet and pure Fe_2O_3 anodes at the current density of 200 $mA \cdot g^{-1}$ for 100 cycles.

The charge/discharge voltage curves of graphene-Fe_2O_3 hybrid sheet electrode were tested at a current density of 200 $mA \cdot g^{-1}$, as shown in Figure 7b. In the first cycle, the discharge/charge capacity was 1466 $mAh \cdot g^{-1}$ and 953 $mAh \cdot g^{-1}$. A high discharge capacity of 1117 $mAh \cdot g^{-1}$ can be attained in the second cycle, with a homologous charge capacity of 893 $mAh \cdot g^{-1}$.

The rate capacities of graphene-Fe_2O_3 hybrid sheet electrodes at diverse current densities are shown in Figure 7c. The graphene-Fe_2O_3 hybrid paper electrode displayed a specific capacity of 495 $mAh \cdot g^{-1}$ even at a high current density of 4 $A \cdot g^{-1}$. Surprisingly, when the current density reset back to 200 $mA \cdot g^{-1}$, it still can deliver a stable capacity of 765 $mAh \cdot g^{-1}$. Therefore, the hybrid paper exhibits extremely complete structure and cycle stability at different current densities.

Figure 7d displays the cyclic performance of graphene-Fe_2O_3 sheet and pure Fe_2O_3 anodes at a constant current density of 200 $mA \cdot g^{-1}$ for 100 cycles. It is obviously observed in the curve that graphene-Fe_2O_3 sheets deliver a higher initial capacity of 1466 $mAh \cdot g^{-1}$ than that of pure Fe_2O_3 anodes (1054 $mAh \cdot g^{-1}$). Stabilized cyclic performance was obtained from the third cycle. Various kinds of Fe_2O_3-graphene powder composites have been shown in Table 1 as a comparison. All the Fe_2O_3-graphene powder composites mentioned in the table are fabricated from the GO aqueous solution and precursors of the transition metal oxide. It is easy to cause the aggregation of graphene during the reduction process with the formation of iron oxide. Therefore, the loading of iron oxide is relatively low (around 30%). Due to the addition of binder and carbon black, the energy density of

the Fe_2O_3-graphene powder composites anode is less than the graphene-Fe_2O_3 sheet anode. At the same current density of 200 $mA \cdot g^{-1}$, the initial capacity of graphene-Fe_2O_3 sheet is 1466 $mAh \cdot g^{-1}$ higher than other references shown in Table 1. After 100 cycles of test, the reversible capacity of graphene-Fe_2O_3 sheet electrode can steadily reach about 765 $mAh \cdot g^{-1}$, which is considerably higher than that of pure Fe_2O_3 (425 $mAh \cdot g^{-1}$) and other graphene-Fe_2O_3 powder composites under the same current density of 200 $mA \cdot g^{-1}$.

Table 1. Anodes for LIBs based on graphene-Fe_2O_3 materials and their electrochemical performance.

Active Material	Current Rate ($mA \cdot g^{-1}$)	Initial Capacity ($mAh \cdot g^{-1}$)	Reversible Capacity ($mAh \cdot g^{-1}$)	Cycle No.	Ref.
Graphene-Fe_2O_3 sheet anode of our work	200	1466	765	100	-
Micro-sized Fe_2O_3 spheres doped with graphene	160	1800	660	100	[28]
α-Fe_2O_3/graphene with 3D quasilaminated architecture	100	1719	742	50	[29]
α-Fe_2O_3/graphene nanocomposites	200	1029	570	20	[30]
Fe_2O_3 particles enwrapped by graphene	50	1544	626	50	[31]
Hierarchically nanospherical α-Fe_2O_3/graphene	100	1442	1024	50	[32]

For investigating the electrochemical properties of electrodes, the EIS measurement was carried out. All Nyquist plots are shown in Figure 8 show two partially overlapping semicircles and a slanted line. The first semicircle in the high-frequency region is in connection with the diffusion of lithium ions through the SEI layer, the second semicircle in the middle-frequency region corresponds to the charge transfer resistance of electrochemical reactions, and the slant line in the low-frequency region is in connection with the solid state diffusion of lithium ions in the bulk electrode [25,33]. After simulation through the equivalent circuit, which is inset in t Figure 8, where Rs represents electrolyte resistance, R_1 and CPE_1 are SEI layer resistors and corresponding capacitors, R_2 and CPE_2 are charge transfer resistors and double layer capacitors, and R_w is volume diffusion resistance [25,34]. As shown in Table 2, the graphene-Fe_2O_3 sheet anode shows a much lower resistance (45.36 Ω) than the reference pure Fe_2O_3 electrode (67.58 Ω), indicating that 3D layered graphene sheets can enhance the electric conductivity [35]. Meanwhile, the results illustrate that the open 3D laminated structure of graphene-Fe_2O_3 hybrid paper exhibits splendid storage capabilities under high current density, attributing to the open layered structure of graphene to cushion the volume changes during the electrochemical process [36]. The EIS results agree fairly well with the electrochemical behaviors.

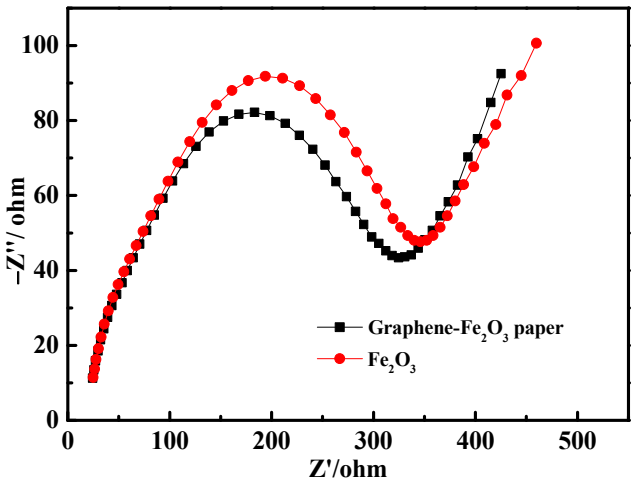

Figure 8. The EIS of the hybrid graphene-Fe_2O_3 sheet anode and Fe_2O_3 anodes before cycling (0.01–100 kHz). Embedded is the modeled equivalent circuit of the EIS.

Table 2. The Nyquist diagram is fitted by the equivalent circuit.

Sample	R_s (Ω)	R_1 (Ω)	CPE_1		R_2 (Ω)	CPE_2	
-	-	-	Y	n	-	Y	n
graphene-Fe_2O_3 paper	2.54	22.89	9.6×10^{-5}	0.84	45.36	4.6×10^{-5}	0.65
Fe_2O_3	4.58	89.26	1.1×10^{-4}	0.92	67.58	5.4×10^{-5}	0.67

4. Conclusions

A novel synthetic route was developed to successfully achieve free-standing graphene-Fe_2O_3 hybrid paper with brilliant electrochemical properties as the anode for LIBs. Fe_2O_3 nanoparticles could be anchored on layered graphene nanosheets used as the pillar to form an open 3D laminated structure. The novel structure is constructed by graphene paper and Fe_2O_3 nanoparticles, which prevent the integration of Fe_2O_3 nanoparticles and provide a void space buffer for the volume changes of Fe_2O_3 nanoparticles during the charge-discharge course. Thus, graphene-Fe_2O_3 hybrid paper electrode shows excellent lithium storing properties and improved cycling properties due to the 3D flexible architecture and the structural integrity. The graphene-Fe_2O_3 hybrid paper electrode can deliver a large reversible capacity of 765 $mAh \cdot g^{-1}$ and high Coulombic efficiency of 99% even after 100 cycles, which indicates the graphene-Fe_2O_3 hybrid paper electrode has a huge potential as the anode for LIBs.

Author Contributions: Conceptualization, C.Y., W.X. and S.R.; writing—original draft preparation, C.Y.; writing—review and editing, C.Y.; supervision, Q.L. All authors have read and agreed to the published version of the manuscript.

Funding: This work was supported by the financial support of the Education Scientific Research Project of Youth Teachers in the Education Department of Fujian Province (contract grant numbers JT180495), the Foundation of Science and Technology of the Sanming Institute of Fluorochemical Industry (contract grant number FCIT20171213), Fujian Key Project of Science and Technology (contract grant number 2121G02012), University Industry Research Cooperation Project of Fujian (contract grant number 2022H6035) and the Scientific Research Foundation for Introducing Talent of Sanming University (contract grant numbers KD180017).

Institutional Review Board Statement: Not applicable.

Informed Consent Statement: Informed consent was obtained from all subjects involved in the study.

Data Availability Statement: Not applicable.

Conflicts of Interest: The authors declare that they have no known competing financial interests or personal relationships that could have appeared to influence the work reported in this paper.

References

1. Wood, D.L.; Li, J.L.; Daniel, C. Prospects for reducing the processing cost of lithium ion batteries. *J. Power Sources* **2015**, *275*, 234–242. [CrossRef]
2. Abazari, S.; Shamsipur, A. Graphene family nanomaterial reinforced magnesium-based matrix composites for biomedical application: A comprehensive review. *Metals* **2020**, *10*, 1002. [CrossRef]
3. Roy, P.; Srivastava, S.K. Nanostructured anode materials for lithium ion batteries. *J. Mater. Chem. A* **2015**, *3*, 2454–2484. [CrossRef]
4. Wang, Z.M.; Xu, X.T.; Kim, J.H.; Malgras, V.; Mo, R.; Li, C.L. Nanoarchitectured metal-organic framework/polypyrrole hybrid for brackish water desalination using capacitive deionization. *Mater. Horiz.* **2019**, *6*, 1433–1437. [CrossRef]
5. Xu, X.T.; Allah, A.E.; Wang, C.; Tan, H.B.; Farghali, A.A.; Khedr, M.H. Capacitive deionization using nitrogen-doped mesostructured carbons for highly efficient brackish water desalination. *Chem. Eng. J.* **2019**, *362*, 887–896. [CrossRef]
6. Adhami, T.; Kahrizsangi, R.E.; Bakhsheshi-Rad, H.R. Synthesis and electrochemical properties of $TiNb_2O_7$ and $Ti_2Nb_{10}O_{29}$ anodes under various annealing atmospheres. *Metals* **2021**, *11*, 983. [CrossRef]
7. Baghbaderani, M.Z.; Abazari, S. Dual synergistic effects of MgO-GO fillers on degradation behavior, biocompatibility and antibacterial activities of chitosan coated Mg alloy. *Coatings* **2022**, *12*, 63. [CrossRef]
8. Ding, Z.B.; Xu, X.T.; Li, Y.Q.; Wang, K.; Lu, T.; Pan, L.K. Significantly improved stability of hybrid capacitive deionization using nickel hexacyanoferrate/reduced graphene oxide cathode at low voltage operation. *Desalination* **2019**, *468*, 114078. [CrossRef]

9. Xu, X.T.; Tang, J.; Kaneti, Y.V.; Tan, H.B.; Chen, T.; Pan, L.K. Unprecedented capacitive deionization performance of interconnected iron–nitrogen-doped carbon tubes in oxygenated saline water. *Mater. Horiz.* **2020**, *7*, 1404–1412. [CrossRef]
10. Wang, G.K.; Sun, X.; Lu, F.Y.; Sun, H.T.; Yu, M.P.; Jiang, W.L. Flexible pillared graphene-paper electrodes for high-performance electrochemical supercapacitors. *Small* **2012**, *6*, 452–461. [CrossRef]
11. Tao, L.Q.; Zhang, K.N.; Tian, H.; Liu, Y.; Wang, D.Y.; Chen, Y.Q. Graphene-paper pressure sensor for detecting human motions. *ACS Nano.* **2017**, *11*, 8790–8795. [CrossRef] [PubMed]
12. Chi, K.; Zhang, Z.Y.; Xi, J.B.; Huang, Y.G.; Xiao, F.; Wang, S. Freestanding graphene paper supported three-dimensional porous graphene–polyaniline nanocomposite synthesized by inkjet printing and in flexible all-solid-state supercapacitor. *ACS Appl. Mater. Interfaces* **2014**, *6*, 16312–16319. [CrossRef] [PubMed]
13. Teng, C.; Xie, D.; Wang, J.F.; Yang, Z.; Ren, G.Y.; Zhu, Y. Ultrahigh conductive graphene paper based on ball-milling exfoliated graphene. *Adv. Funct. Mater* **2017**, *27*, 1700240. [CrossRef]
14. Xu, X.T.; Yang, T.; Zhang, Q.W.; Xia, W.; Ding, Z.B.; Eid, K. Ultrahigh capacitive deionization performance by 3D interconnected MOF-derived nitrogen-doped carbon tubes. *Chem. Eng. J.* **2020**, *390*, 124493. [CrossRef]
15. Huang, H.J.; Yan, M.M.; Yang, C.Z.; He, H.Y.; Jiang, Q.G.; Yang, L. Graphene nanoarchitectonics: Recent advances in graphene-based electrocatalysts for hydrogen evolution reaction. *Adv. Mater* **2019**, *31*, 1903415. [CrossRef]
16. Liu, Y.H.; Zeng, J.; Han, D.; Wu, K.; Yu, B.W.; Chai, S.G. Graphene enhanced flexible expanded graphite film with high electric, thermal conductivities and EMI shielding at low content. *Carbon* **2018**, *133*, 435–445. [CrossRef]
17. Xu, X.T.; Liu, Y.L.; Wang, M.; Zhu, C.; Lu, T.; Zhao, R.; Pan, L. Hierarchical hybrids with microporous carbon spheres decorated three-dimensional graphene frameworks for capacitive applications in supercapacitor and deionization. *Electrochim. Acta.* **2016**, *193*, 88–95. [CrossRef]
18. Shi, Q.R.; Cha, Y.W.; Song, Y.; Lee, J.I.; Zhu, C.Z.; Li, X.Y. 3D graphene-based hybrid materials: Synthesis and applications in energy storage and conversion. *Nanoscale* **2016**, *8*, 15414–15447. [CrossRef]
19. Peng, S.J.; Li, L.L.; Lee, J.K.Y.; Tian, L.L.; Srinivasan, M.; Adams, S. Electrospun carbon nanofibers and their hybrid composites as advanced materials for energy conversion and storage. *Nano Energ.* **2016**, *22*, 361–395. [CrossRef]
20. Wang, R.H.; Xu, C.H.; Sun, J.; Gao, L. Three-dimensional Fe_2O_3 nanocubes/nitrogen-doped graphene aerogels: Nucleation mechanism and lithium storage properties. *Sci. Rep.* **2015**, *4*, 7171. [CrossRef]
21. Wang, M.; Wang, G.; Wang, H. Flexible free-standing Fe_2O_3/graphene/carbon nanotubes hybrid filmsas anode materials for high performance lithium-ion batteries. *Electrochimi. Acta.* **2015**, *182*, 192–201. [CrossRef]
22. Sahoo, M.; Sreena, K.P.; Vinayan, B.P.; Ramaprabhu, S. Green synthesis of boron doped graphene and its application as high performance anode material in Li ion battery. *Mater. Res. Bull.* **2015**, *61*, 383–390. [CrossRef]
23. Liang, J.J.; Xu, Y.F.; Sui, D.; Zhang, L.; Huang, Y.; Ma, Y.F. Flexible, magnetic, and electrically conductive graphene/Fe3O4 paper and its application for magnetic-controlled switches. *J. Phys. Chem. C* **2010**, *114*, 17465–17471. [CrossRef]
24. Yu, G.H.; Hu, L.B.; Vosgueritchian, M.; Wang, H.L.; Xie, X.; McDonough, J.R. Solution-processed graphene/MnO_2 nanostructured textiles for high-performance electrochemical capacitors. *Nano Lett.* **2011**, *11*, 2905–2911. [CrossRef] [PubMed]
25. Jaroonwatana, W.; Theerathanagorn, T.; Theerasilp, M.; Gobbo, S.; Yiamsawas, D. Nanoparticles of aromatic biopolymers catalyze CO2 cycloaddition to epoxides under atmospheric conditions. *Sustain. Energ. Fuels* **2021**, *5*, 5431–5444. [CrossRef]
26. Hu, T.; Sun, X.; Sun, H.T.; Yu, M.P.; Lu, F.Y.; Liu, C.S. Flexible free-standing graphene-TiO_2 hybrid paper for use as lithium ion battery anode materials. *Carbon* **2013**, *51*, 322–326. [CrossRef]
27. Li, G.R.; Lei, W.; Luo, D.; Deng, Y.P.; Wang, D.L.; Chen, Z.W. 3D porous carbon sheets with multidirectional ion pathways for fast and durable lithium-sulfur batteries. *Adv. Energy Mater.* **2017**, *8*, 17023. [CrossRef]
28. Hu, T.; Xie, M.; Zhong, J.; Sun, H.T.; Sun, X.; Scott, S. Porous Fe_2O_3 nanorods anchored onnitrogen-doped graphenes and ultrathin Al_2O_3 coating by atomic layer deposition for long-lived lithium ion battery anode. *Carbon* **2014**, *76*, 141–147. [CrossRef]
29. Xiao, L.; Wu, D.Q.; Han, S.; Huang, Y.S.; Li, S.; He, M.Z. Self-assembled Fe_2O_3/graphene aerogel with high lithium storage performance. *ACS Appl. Mater. Interfaces* **2013**, *5*, 3764–3769. [CrossRef]
30. Chen, D.Z.; Wei, W.; Wang, R.N.; Zhu, J.C.; Guo, L. α-Fe_2O_3 nanoparticles anchored on graphene with 3D quasi-laminated architecture: In situ wet chemistry synthesis and enhanced electrochemical performance for lithium ion batteries. *New J. Chem.* **2012**, *36*, 1589–1595. [CrossRef]
31. Xue, X.Y.; Ma, C.H.; Cui, C.X.; Xing, L.L. High lithium storage performance of α-Fe_2O_3/graphene nanocomposites as lithium-ion battery anodes. *Solid State Sci.* **2011**, *13*, 1526–1530. [CrossRef]
32. Xiao, W.; Wang, Z.X.; Guo, H.J.; Li, X.H.; Wang, J.X.; Huang, S.L. Fe_2O_3 particles enwrapped by graphene with excellent cyclability and rate capability as anode materials for lithium ion batteries. *Appl. Surf. Sci.* **2013**, *266*, 148–154. [CrossRef]
33. Lian, X.B.; Cai, M.C.; Qin, L.L.; Cao, Y.; Wu, Q.H. Synthesis of hierarchical nanospheres Fe_2O_3 /graphene composite and its application in lithium-ion battery as a high-performance anode material. *Ionics* **2016**, *22*, 2015–2020. [CrossRef]
34. Petnikota, S.; Marka, S.K.; Banerjee, A.; Reddy, M.V.; Srikanth, V.V.S.S.; Chowdari, B.V.R. Graphenothermal reduction synthesis of 'exfoliated graphene oxide/iron (II) oxide' composite for anode application in lithium ion batteries. *J. Power Sources* **2015**, *293*, 253–263. [CrossRef]

35. Yang, J.; Zhang, Y.; Sun, C.C.; Liu, H.Z.; Li, L.Q.; Si, W.L. Graphene and cobalt phosphide nanowire composite as an anode material for high performance lithium-ion batteries. *Nano. Res.* **2016**, *9*, 612–621. [CrossRef]
36. Ma, L.; Zhou, X.P.; Xu, L.M.; Xu, X.Y.; Zhang, L.L.; Chen, W.X. Ultrathin few-layered molybdenum selenide/graphene hybrid with superior electrochemical Li-storage performance. *J. Power Sources* **2015**, *285*, 274–280. [CrossRef]